Removal of Heavy Metal Ions Using a Functionalized Single-Walled Carbon Nanotube: A Molecular Dynamics Study

ARTICLE *in* THE JOURNAL OF PHYSICAL CHEMISTRY A · JULY 2015

Impact Factor: 2.69 · DOI: 10.1021/acs.jpca.5b03352 · Source: PubMed

3 AUTHORS, INCLUDING:

Anitha Kommu
Indian Institute of Technology Kanpur
1 PUBLICATION **1** CITATION
SEE PROFILE

Sadanandam Namsani
Indian Institute of Technology Kanpur
4 PUBLICATIONS **3** CITATIONS
SEE PROFILE

THE JOURNAL OF PHYSICAL CHEMISTRY A

Article

pubs.acs.org/JPCA

Removal of Heavy Metal Ions Using a Functionalized Single-Walled Carbon Nanotube: A Molecular Dynamics Study

K. Anitha, Sadanandam Namsani, and Jayant K Singh*

Department of Chemical Engineering, Indian Institute of Technology Kanpur, Kanpur, UP-208016, India

ABSTRACT: The adsorption behaviors of heavy metal ions Cd^{2+}, Cu^{2+}, Pb^{2+}, and Hg^{2+}, in aqueous media using functionalized single-walled carbon nanotube (SWCNT) with functional groups $-COO^-$, $-OH$, and $-CONH_2$ are studied using molecular dynamics (MD) simulations. The results show that adsorption capacity is improved significantly using surface modification of SWCNT with carboxyl, hydroxyl, and amide functional groups. In addition, the adsorption capacity is found to increase with increasing metal-ion concentration. It is observed that the $CNT-COO^-$ surface effectively adsorbs over 150−230% more metal ions than the bare CNT surface. On the contrary, $-OH$ and $-CONH_2$ are relatively weak functional groups where excess metal-ion adsorption compared to the bare CNT is in the range 10−47%. The structural properties, self-diffusion coefficients, and adsorption isotherms of the metal ions are computed and analyzed in detail. Moreover, the potential of mean force (PMF) is computed to understand the free energy of metal ions, in the presence of functional groups, which is remarkly higher in absolute terms, leading to significant affinity for adsorption compared to the case for the bare CNT. In general, the following order of adsorption of the metal ions on functionalized CNT is observed: $Pb^{2+} > Cu^{2+} > Cd^{2+} > Hg^{2+}$.

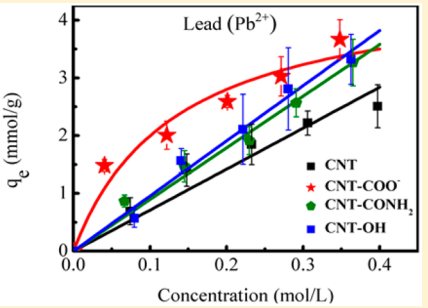

1. INTRODUCTION

Natural water resources are polluted with variety of metal ions such as cobalt (Co), copper (Cu), iron (Fe), manganese (Mn), molybdenum (Mo), vanadium(V), strontium (Sr), and zinc (Zn) by wastewater discharged from industries such as smelting, metal plating, phosphate fertilizer, mining, galvanizing, paints, pigments, cosmetics, and alloy manufacturing.[1] Exposure to these contaminants in water causes adverse health effects on various forms of life.[2−4] Hence, it is crucial to remove the metal ions from effluents discharged from various industries.

Numerous methods are being used for removal of metal ions that include ion exchange, solvent extraction, chemical precipitation, ultrafiltration, and adsorption.[5−7] Although wastewater treatment techniques used for removal of metal ions can be employed for that of heavy metals ions, they have their inherent advantages and limitations. The chemical precipitation method is usually adopted to treat wastewater containing a high concentration heavy metal ions. But it is ineffective when the metal-ion concentration is low.[8−10] However, chemical precipitation is not economical and can produce a large amount of sludge. On the contrary ion exchange has been widely applied for removal of heavy metal from wastewater. However, ion-exchange resins must be regenerated by chemical reagents when they are exhausted, which can cause serious secondary pollution.[11−13] Further, it is expensive, especially when a large amount of wastewater containing heavy metal is treated at low concentration, which makes it impractical for large scale applications. Membrane filtration technology can remove heavy metal ions with high efficiency; its problem such as high cost, complexity of the process, fouling, and low permeate flux have limited their use for the removal of heavy metals.[14−16] Among various methods for removal of metal ions from aqueous solutions, the adsorption based method is more versatile and widely used process.[17] Many varieties of low-cost adsorbents have been developed and tested to remove heavy metal ions. Types of adsorbents used for the adsorption of metal ions are sawdust, zeolites, montmorillonites, activated carbon (AC), wood char, biomass and granulated activated carbon.

Recently, carbon nanotubes (CNTs) have demonstrated high capacity for adsorbing a wide variety of heavy metal pollutants.[18] CNTs have proved to possess great potential for removing heavy metal ions such as lead,[19,20] cadmium,[21] chromium,[22] copper,[23] and nickel[24] from wastewater. CNT exists as single-walled CNT (SWCNTs) or multiwalled CNT (MWCNT).[25,26] Both kinds of CNTs are used in adsorption, and MWCNTs became popular because their synthesis is cheaper and they are easy to synthesize. However, the experimental results for adsorption of divalent metal ions on SWCNTs and MWCNTs showed that SWCNTs has over 18% higher adsorption capacity than MWCNTs.[27,28] The surface nature of CNT can be modified using chemical and thermal treatment. The large number of experimental studies has been devoted to metal-ion adsorption on bare and functionalized CNTs. Recent experiments used armchair (6, 6) CNT functionalized with carboxyl (−COOH), carbonyl (−CO), and hydroxyl (−OH) groups to study the metal-ion adsorption.

Received: April 7, 2015
Revised: July 8, 2015
Published: July 9, 2015

DOI: 10.1021/acs.jpca.5b03352
J. Phys. Chem. A 2015, 119, 8349−8358

These experimental investigations showed that the metal-ion adsorption capacity on CNT surface is improved after modification.[27,29−32] The mechanism by which the metal ions are sorbed onto CNTs are intricate and has been attributed to electrostatic attraction, sorption−precipitation and chemical interaction between metal ions and surface functional groups of CNTs.[28] However, it is observed that CNT surface properties, solution pH, and temperature can affect the adsorption process. The percentage of adsorbed metal ion on the CNT increases with increasing temperature of the system. This is attributed to the higher diffusion rate of metal ions and lower activation energy of sorption at higher temperatures.[27,33−36] The pH of the solution is also an important parameter in the adsorption process. Many experimental results[33,37−40] showed that at low pH (2−7) the rate of adsorption is low, and at high pH (8−11) the rate of adsorption increases. There are only few theoretical studies on the adsorption of heavy metal ions on armchair type of SWCNTs. The simulations by Ansari and co-workers[41−43] have suggested that the adsorption of Zn(II) on the surface of armchair SWCNT (6, 6) gets affected by temperature, pH, and surface modification of CNTs. The authors also explored the effect of charged CNTs on adsorption of Zn(II) and Cd(II) ions using molecular dynamics (MD) approach. It was shown that the Cd(II) adsorption rate increases with increasing the net CNT surface charge from −0.01 to −0.02e. On the contrary, the Zn(II) adsorption rate was reported to decrease with increasing net CNT charge. However, not much is known, to our best knowledge, about the adsorption behavior of other divalent metal ions in the presence of pure or functionalized CNTs.

The present study is aimed to investigate the adsorption behavior of divalent metal ions viz., Cd^{2+}, Cu^{2+}, Pb^{2+}, and Hg^{2+} ions onto bare and functionalized CNT surfaces from aqueous solution using MD simulations. The rest of the paper is organized as follows. In section 2, the interaction potentials used for carbon nanotube, water, nitrate, and metal ions are described briefly along with the simulation details. In section 3, the results and discussion presents the density profiles of metal ions, which explain the ion distribution around CNTs. The adsorption isotherm, self-diffusion coefficient, and residence time distribution of metal ions of variable concentration on CNT surface are also investigated in detail. The role of functionalization is analyzed in terms of radial distribution function, diffusion coefficients, and potential of mean force (PMF). Conclusion is drawn in section 4.

2. MODELS AND METHODS

In this study, an armchair type (6, 6) SWCNT with a diameter of 8.14 Å and length of 24.5 Å is considered. All the MD simulations are performed on a system consisting of SWCNT solvated in various aqueous concentrations of $Cd(NO_3)_2$, $Cu(NO_3)_2$, $Pb(NO_3)_2$, and $Hg(NO_3)_2$ ionic salts. TIP3P model[44] is used to model water interactions, and OPLS (optimized potential for liquid simulation) parameters are used for metal ions, CNTs, and functional groups ($-COO^-$, $-OH$ and $-CONH_2$).[45,46] The force field parameters used in this work are tabulated in Table 1. The carbon atoms in CNTs are modeled as uncharged and kept rigid.

The nonbonded interactions of water and ions with CNT are described by eq 1.

Table 1. Potential Parameters

molecules/ions	site	charge (e)	σ (Å)	ε (kcal/mol)
water	O (water)	−0.8340	3.1506	0.1521
	H (water)	0.4170	0.000	0.0000
CNT	C	0.000	3.400	0.086
$-COO^-$	C(CNT)	0.100	3.400	0.086
	C(FG)	0.700	3.750	0.109
	O(C═O)	−0.800	2.960	0.210
	O(C—O^-)	−1.000	2.960	0.210
$-OH$	C(CNT)	0.200	3.400	0.086
	O	−0.640	3.070	0.155
	H	0.440	0.000	0.000
$-CONH_2$	C(CNT)	0.100	3.400	0.086
	C(FG)	0.700	3.750	0.105
	O(C═O)	−0.800	2.960	0.210
	N	−0.760	3.250	0.170
	H	0.380	0.000	0.000
$-NO_3^-$	N	0.950	3.207	0.160
	O	−0.650	3.349	0.170
metal ions	Pb^{2+}	2.000	3.000	0.19112
	Cd^{2+}	2.000	2.700	0.00597
	Cu^{2+}	2.000	2.130	0.0500
	Hg^{2+}	2.000	2.360	0.0409

$$U_{\text{nonbond}} = 4\varepsilon_{ij}\left[\left(\frac{\sigma_{ij}}{r_{ij}}\right)^{12} - \left(\frac{\sigma_{ij}}{r_{ij}}\right)^{6}\right] + \frac{q_i q_j}{4\pi\varepsilon_0 r_{ij}} \quad (1)$$

where ε_{ij} and σ_{ij} are the energy and length parameters of Lennard-Jones potential, respectively. The charge on the atoms i and j are represented by q_i and q_j, respectively, and r_{ij} denotes center to center distance; here ε_0 denotes the dielectric permittivity constant.

All the stretching and bending interactions in the nitrate ions are modeled using harmonic potentials:

$$U_{\text{bond}} = \frac{1}{2}k_r(r - r_{\text{eq}})^2 \qquad U_{\text{angle}} = \frac{1}{2}k_\theta(\theta - \theta_{\text{eq}})^2 \quad (2)$$

Cross interaction parameters of unlike pairs of i and j particles were calculated by using Lorentz−Berthelot mixing rules,[47] for which the C−C interaction is described using the Lennard-Jones potential with parameters[48−52] σ_{cc} = 3.4 Å and ε_{cc} = 0.086 kcal/mol.

All MD simulations are carried out using LAMMPS package.[53] The simulations are performed with CNT solvated in five different concentrations (0.1, 0.2, 0.3, 0.4, and 0.5 M) for each metal ion using their nitrate salt ($Cd(NO_3)_2$, $Cu(NO_3)_2$, $Pb(NO_3)_2$, and $Hg(NO_3)_2$) in an aqueous medium. A representative snapshot is shown in Figure 1. An orthogonal simulation box (63.0 × 63.0 × 29.0 $Å^3$) is used containing one CNT aligned along the z-axis. Subsequently, water (3703) molecules and metal ions are added to the simulation box with the help of Packmol program.[54] Periodic boundary conditions are applied in all directions. Long-range electrostatic interactions are accounted using particle—particle particle—mesh (PPPM) technique as implemented in LAMMPS. A cutoff distance of 10 Å is used for the nonbonded interactions. A time step of 1.0 fs is used, and trajectories of the simulations are collected for every 10 ps for analysis.

The simulation system is first equilibrated using a constant pressure and temperature (*NPT*) ensemble at 298 K and 1 atm for 1 ns. The temperature and pressure of the system are

DOI: 10.1021/acs.jpca.5b03352
J. Phys. Chem. A 2015, 119, 8349−8358

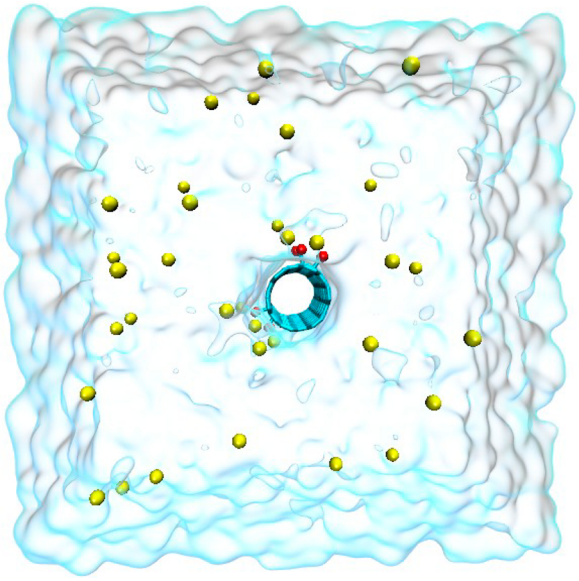

Figure 1. Representative simulation system with a 0.5 M salt concentration and a CNT functionalized with a $-COO^-$ group. Cyan and red colors represent carbon and oxygen atoms of the functional CNT. Water is represented as a light blue surface, and metal ions are shown in yellow.

maintained using Nosé–Hoover thermostat and barostat.[55,56] Further, we have used the equilibrium configurations from *NPT* simulations, of different metal-ion systems, to perform 50 ns constant volume and temperature (*NVT*) ensemble simulations at 298 K using a Nosé–Hoover thermostat. The trajectories of the system obtained from *NVT* simulations are used to calculate the adsorption capacity of ions on CNT. Although pH of most of the wastewater streams is ~6.0, we have performed simulations for neutral system at a pH of 7.

The normalized radial density profiles ($\rho/\rho_0(r)$) are calculated from the center line of the CNT for the metal ions for five different concentrations. The occupation time distribution function of metal ion is calculated using the time correlation function $R(t)$, as shown in eq 3. The residence time (τ_s) is evaluated by fitting an exponential form, as shown in eq 4, to the $R(t)$ values.

$$R(t) = \frac{\langle \sum_{i=1}^{N} \theta_i(t_0)\, \theta_i(t + t_0) \rangle}{\langle \sum_{i=1}^{N} \theta_i(t_0)\, \theta_i(t_0) \rangle} \tag{3}$$

$$R(t) = A \exp[-(t/\tau_s)] \tag{4}$$

The diffusion coefficients of metal ions are calculated from mean-square displacement (MSD) using eqs 5 and 6.

$$\mathrm{MSD}(t) = \frac{1}{N} \sum_{i=1}^{N} (|r_i(t+\Delta t) - r_i(t)|)^2 \tag{5}$$

$$D = \frac{1}{6} \lim_{t\to\infty} \frac{\mathrm{d}}{\mathrm{d}t}(\mathrm{MSD}) \tag{6}$$

where $r_i(t)$ is the vector position of the atom i at time t. N is the number of atoms of the divalent metal ions.

Adsorption equilibrium is described with the Langmuir isotherm:

$$q_e = \frac{q_{max} KC}{1 + KC} \tag{7}$$

where q_e is the amount of metal ion adsorbed per unit mass of CNT (mmol/g). q_{max} (mmol/g) is the maximum amount of metal ion adsorbed, and K is the constant. The concentration (C, mol/L) is the equilibrium concentration of ion in the solution.

3. RESULTS AND DISCUSSION

Structural Properties of Heavy Metal Ions. The normalized radial density distributions of cadmium (Cd^{2+}) ions from the center line of the bare and functionalized CNTs at 0.1, 0.2, 0.3, 0.4, and 0.5 M concentrations are shown in Figure 2a–e, respectively. The first peak heights of the radial

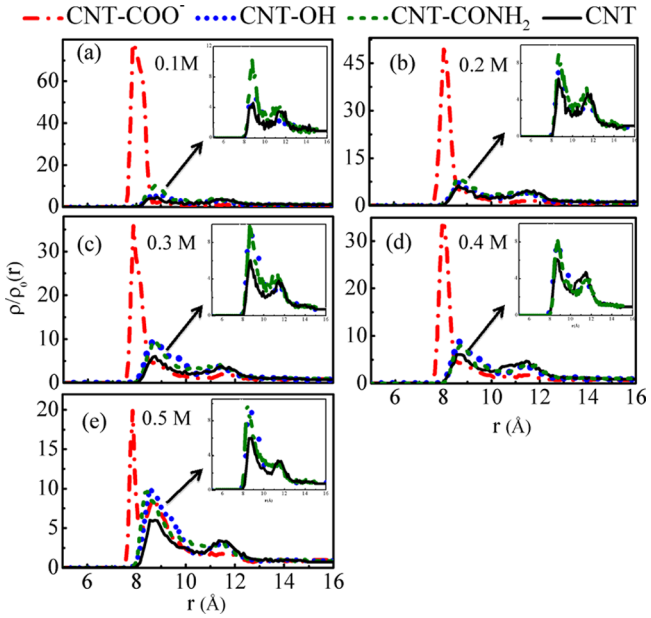

Figure 2. Normalized radial density profiles of Cd^{2+} from the center line of CNT with different functional groups at (a) 0.1 M, (b) 0.2 M, (c) 0.3 M, (d) 0.4 M, and (e) 0.5 M ion concentrations. The inset shows the zoomed in view of the profile, which illustrates that the peak height corresponding to the functionalized CNTs ($-OH$ and $-CONH_2$) is higher than that of the bare CNT.

density profiles for functionalized CNTs are substantially pronounced compared to that of the bare CNT, which is much more evident at lower concentration. In general, among the functional groups, the $-COO^-$ group on the CNT surface displays remarkably better adsorption of ions than the $-OH$ and $-CONH_2$ functional groups on the CNT surface, which is clearly evident from the pronounced first peak of the distribution at all concentrations studied in this work. Though the $-COO^-$ groups retains its superior adsorption behavior, the relative affinity of other groups ($-OH$ and $-CONH_2$) with the Cd^{2+} ion significantly increases with increasing concentration as apparent from the increased first peak of the radial density distribution. Interestingly, at all concentrations, the first peak position of the radial density profiles for Cd^{2+} ion in the presence of carboxylic functional group on the CNT surface is at ~8.0 Å, as opposed to the first peak position at ~9.0 Å seen in the presence of other groups.

Figure 3 presents typical snapshots of Cd^{2+} ions in the presence of different functional groups. It is evident from the

DOI: 10.1021/acs.jpca.5b03352
J. Phys. Chem. A 2015, 119, 8349–8358

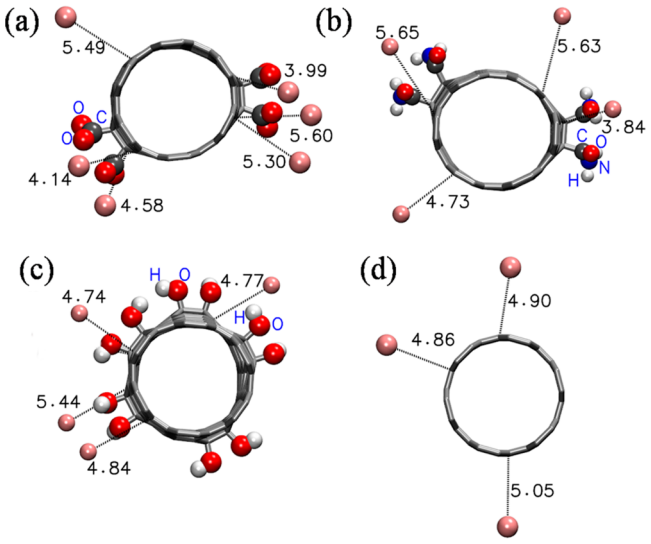

Figure 3. Snapshots of cadmium (Cd^{2+}) ion with functionalized CNT and bare CNT at 0.5 M concentration within a cutoff distance, 10 Å, from the center line of CNT (a) CNT−COO^-, (b) CNT−$CONH_2$, (c) CNT−OH, and (d) bare CNT.

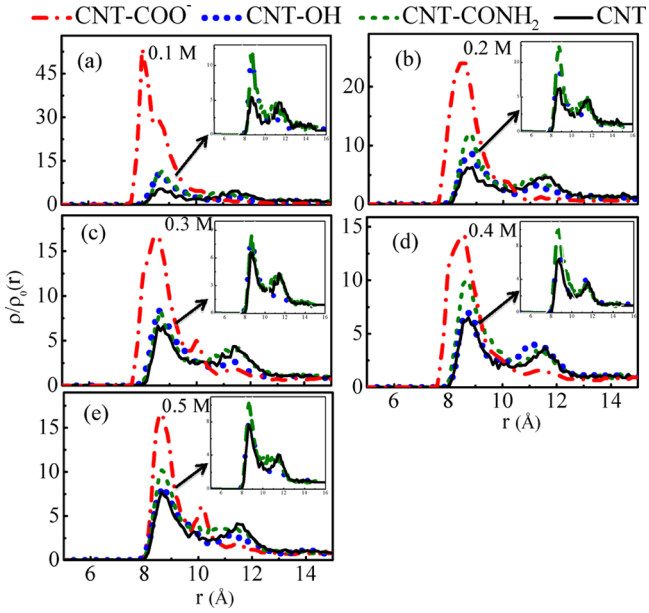

Figure 4. Normalized radial density profiles of Cu^{2+} from the center line of CNT with different functional groups at (a) 0.1 M, (b) 0.2 M, (c) 0.3 M, (d) 0.4 M, and (e) 0.5 M ion concentrations. The inset shows the zoomed in view of the profile, which illustrates that the peak height corresponding to the functionalized CNTs (−OH and −$CONH_2$) is higher than that of the bare CNT.

snapshots that more Cd^{2+} ions are closer to the CNT surface in the presence of the −COO^- group. The heights of the density profile peaks are different in the presence of functional groups and bare CNT. The higher peak height for the case of CNT−COO^- (Figure 3a) is due to higher affinity of cadmium ions in the presence of CNT−COO^- compared to that for CNT−$CONH_2$ (Figure 3b), CNT−OH (Figure 3c), and bare CNT (Figure 3d). This is also reflected in the snapshots, where the number of ions for −COO^-, −$CONH_2$, and −OH are 6, 4, and 4, respectively. This is further supported by the PMF values of different functional groups, which is described in a later section. The position of the peaks in the radial density profiles (Figure 2) does not change with increasing concentration. However, the height of the peak is sensitive to the ion concentration. There is another noteworthy observation. Although the normalized densities of the Cd^{2+} with −OH and −$CONH_2$ show weaker first peak relative to −COO^- group, the second peak is relatively more pronounced, which appears at ∼11.50 Å (Figure 2e). This is contrary to the case of −COO^- where the second peak coincides with the first peak of other groups. The adsorption capacity of Cd^{2+} ion on the CNT surface based on the radial density profile is observed to follow the order CNT−COO^- > CNT−$CONH_2$ ≈ CNT−OH > bare CNT.

The normalized radial density distribution of Cu^{2+} metal ion from the center line of the bare and functionalized CNTs at different concentrations is shown in Figure 4. Akin to the behavior seen for Cd^{2+}, the first peak height of the normalized radial density profile of the copper metal ion is significantly higher in the presence of the carboxylic functional group on the CNT surface than with the hydroxyl or amide functional groups on the CNT surface and bare CNT. The large peak height shows an increased affinity of the CNT surface to adsorb more metal ions on the surface. Moreover, other functional groups, −OH and −$CONH_2$, also display higher peak heights than the bare CNT. This shows that the metal-ion adsorption capacity of functionalized CNT (−COO^-, −OH, and −$CONH_2$) is significantly more than the bare CNT. For all concentrations of the Cu^{2+} ion, the first peak position of metal ion is around 8.5 Å from the center line of the CNT for both functionalized CNTs and bare CNT. The peak height of the normalized radial density profile of metal ion is different for various functional groups on the CNT surface indicative of differences in their affinity toward the metal ions.

Figure 5 presents the corresponding snapshots for illustration, where it is evident that copper ions prefer to be closer to the CNT surface for all functional groups (−COO^-, −OH, and −$CONH_2$) than to the bare CNT. However, the count of copper ions adsorbed on the CNT surface varies with functional groups. For example, at 0.5 M the number of Cu^{2+}

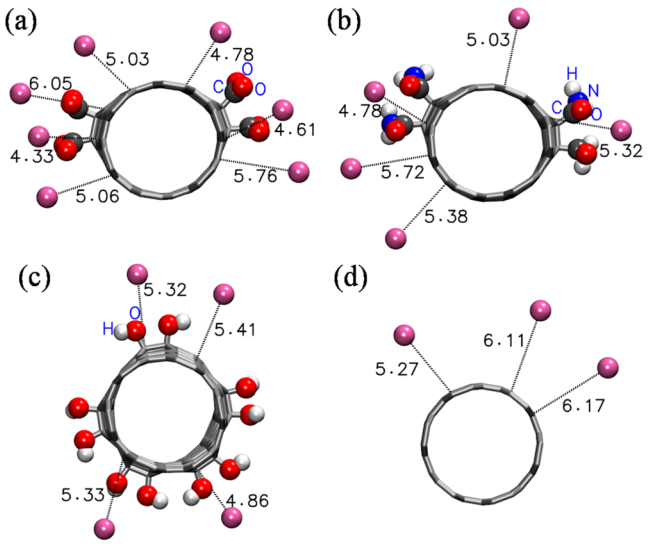

Figure 5. Snapshots of copper (Cu^{2+}) ion with functionalized CNT and bare CNT at 0.5 M concentration with a cutoff 10 Å from the center line of CNT (a) CNT−COO^-, (b) CNT−$CONH_2$, (c) CNT−OH, and (d) bare CNT.

DOI: 10.1021/acs.jpca.5b03352
J. Phys. Chem. A 2015, 119, 8349−8358

ions in the presence of $-COO^-$, $-CONH_2$, and $-OH$ groups on the CNT surface are 7, 5, and 4, respectively. Hence, based on the normalized radial density profile function, the order of Cu^{2+} ion adsorption capacity on the CNT surface is CNT$-COO^-$ > CNT$-CONH_2$ > CNT$-$OH > bare CNT.

In addition to Cd^{2+} and Cu^{2+}, adsorption of Pb^{2+} ions on bare and functionalized CNTs at different concentrations is carried out. The normalized radial density profiles from the center line of CNT at different concentrations of $Pb(NO_3)_2$ are given in Figure 6. Similar to the peak heights for other metal

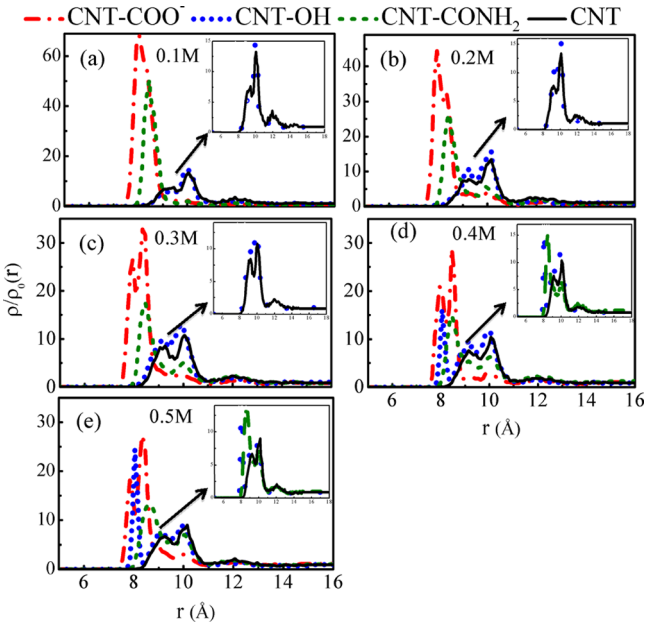

Figure 6. Normalized radial density profiles of Pb^{2+} from the center line of CNT with different functional groups at (a) 0.1 M, (b) 0.2 M, (c) 0.3 M, (d) 0.4 M, and (e) 0.5 M ion concentrations. The inset shows the zoomed in view of the profile, which illustrates that the peak height corresponding to the functionalized CNTs ($-OH$ and $-CONH_2$) is higher than that of the bare CNT.

ions considered in this work, the peak height of the Pb^{2+} normalized radial density profile in the presence of the $-COO^-$ functional group is higher than those for the bare CNT and other $-OH$ and $-CONH_2$ functionalized CNTs. This shows that the $-COO^-$ group functionalized on the CNT surface exhibits better adsorption capacity than the bare and other functionalized CNTs, akin to that seen for other metal ions. Moreover, the peak heights of the radial density profile of lead ion for CNT surface functionalized with $-OH$ and $-CONH_2$ functional groups, though of similar order, are higher than the bare CNT. Hence, functionalized CNTs give better adsorption characteristics than bare CNT for Pb^{2+}. For all salt concentrations, the $-COO^-$ group functionalized CNT shows better Pb^{2+} ion adsorption capacity than the other functional groups attached to CNT, which is evident from the larger peak heights in Figure 6. The normalized radial density of Pb^{2+} ions from the center line of CNT$-COO^-$, at low concentrations, 0.1 and 0.2 M (Figure 6a,b), shows a single peak at 8.3 Å. At higher concentrations, 0.3, 0,4 and 0.5 M (Figure 6c–e) the peak splits such that the first peak is at 7.7 Å and the second peak remains at 8.3 Å.

This indicates that the lead ions form a single coordination shell at lower concentrations (0.1 and 0.2 M). With an increase in the metal-ion concentration (0.3, 0.4, and 0.5 M), two coordination shells are observed within 10 Å. This shows that more lead ions are nearer to the CNT surface due to the effect of the $-COO^-$ functional group on the CNT surface (Figure 7). In the case of other functional groups ($-OH$ and

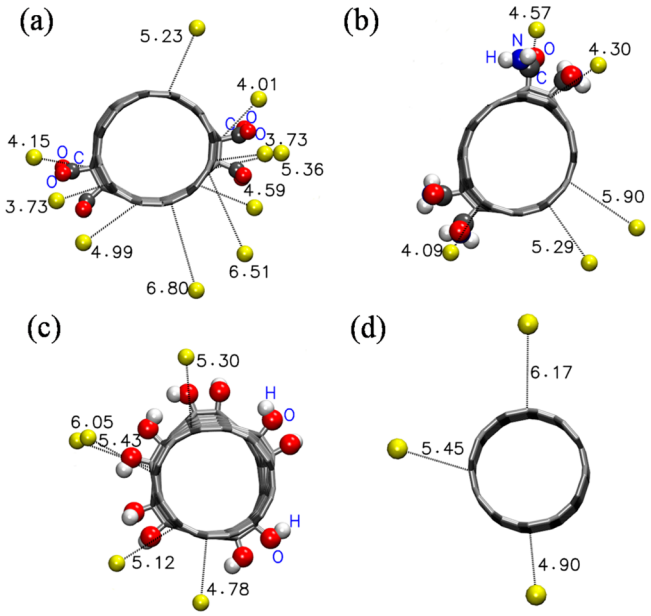

Figure 7. Snapshots of lead (Pb^{2+}) ion with functionalized CNT and bare CNT at 0.5 M concentration with in a 10 Å cutoff from the center line of CNT (a) CNT$-COO^-$, (b) CNT$-CONH_2$, (c) CNT$-$OH, and (d) bare CNT.

$-CONH_2$) and bare CNT the normalized radial density peak positions are shifted away from the CNT surface. The amide functional group on the CNT surface shows only a single peak within 10 Å, at all ion concentrations. For the case of CNT surface functionalized with hydroxyl group (CNT$-$OH), low lead ion concentration (0.1, 0.2, and 0.3 M) systems show a single peak at 9 Å (Figure 6a–c). However, for higher concentrations, 0.4 and 0.5 M, the normalized radial density of the Pb^{2+} ion displays two peaks, at 7.7 and 9 Å (Figure 6d,e). Although bare CNT display some affinity for metal ions, the peak position is relatively away from the surface as opposed to that seen for functional groups. Moreover, in the case of functionalized CNT compared to bare CNT (Figure 7) the peak heights of the density profiles are higher because more ions are near the surface. Furthermore, it is evident from Figure 7 that the CNT surface in the presence of the carboxylic functional group has a higher adsorption capacity for Pb^{2+} ions than the hydroxyl and amide functional groups and bare CNT. For example, at 0.5 M, the numbers of ions adsorbed on the CNT surface in the presence of $-COO^-$, $-CONH_2$, and $-OH$ groups are 10, 5, and 5, respectively. Hence, based on the above analysis, the order of Pb^{2+} ion adsorption capacity on the CNT surface is CNT$-COO^-$ > CNT$-$OH ≈ CNT$-CONH_2$ > bare CNT.

Adsorption Isotherms. To this end, we calculate adsorption isotherm of bare and functionalized CNTs for the four metal ions at different concentrations, which are presented in Figure 8, for Cd^{2+}, Cu^{2+}, Pb^{2+}, and Hg^{2+}, respectively. The adsorption isotherm is fitted with the Langmuir isotherm equation. Table 2 summarizes the parameters obtained from the fitting of adsorption isotherm.

DOI: 10.1021/acs.jpca.5b03352
J. Phys. Chem. A 2015, 119, 8349–8358

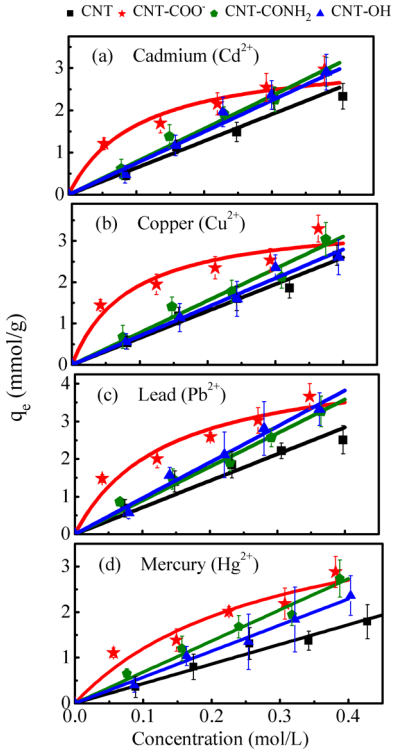

Figure 8. Langmuir adsorption isotherm showing the variation of total amount of metal ion adsorbed (q_e) with the concentration (mol/L) for adsorption of (a) Cd^{2+}, (b) Cu^{2+}, (c) Pb^{2+}, and (d) Hg^{2+} ions onto functionalized CNT and bare CNT.

The adsorption isotherms are found to fit eq 7 extremely well, with correlation coefficient (R^2) close to 1, indicating that the adsorption of divalent metals ions on the CNT surface follows the Langmuir's model. Figure 8 shows the graphical comparison of the simulated data of metal-ion adsorption on functionalized CNT ($-COO^-$,$-OH$, and $-CONH_2$) and bare CNT, which are in agreement with calculated Langmuir isotherm data. The maximum adsorption capacities of Cd^{2+}, Cu^{2+}, Pb^{2+}, and Hg^{2+} on the functionalized CNT surface ($-COO^-$, $-OH$, and $-CONH_2$), calculated from the Langmuir isotherm equation, follow the order $Pb^{2+} > Cu^{2+} > Cd^{2+} > Hg^{2+}$. The adsorption of Pb^{2+} ions on CNT surface is more than the other metal ions (Cu^{2+}, Cd^{2+}, and Hg^{2+}) for all the salt concentrations studied in this work. The highest monolayer adsorption capacities for Pb^{2+}, Cu^{2+}, Cd^{2+}, and Hg^{2+} ions are found to be 4.672, 3.565, 3.325, and 3.300 mmol/g, respectively, on the CNT$-COO^-$ surface. The $-COO^-$ group increases the maximum amount of adsorption of Pb^{2+}, Cu^{2+}, Cd^{2+}, and Hg^{2+} by ~230%, 190%, 150%, and 175% compared to the case of the bare CNT. The results are compared with the experimental results available in the literature[28,32] and found to be in good agreement. Few experimental studies[32] have shown that the ζ potential of the CNT surface becomes more negative than that for the bare CNT after modification of CNT with functional groups. Ansari et al.[41−43] performed adsorption studies of Zn^{2+} ion on SWCNT using MD simulations. The authors reported that the maximum amount of metal ions adsorbed per gram of functionalized CNT is higher for the carboxyl group than for the hydroxyl functionalized CNT and bare CNT. Further, the authors found that increasing the surface charges increases the adsorption capacity. Our results on the adsorption capacity of metal ions on functional groups are akin to that seen in the literature. Some MD simulation studies demonstrated that CNT functionalized with carboxyl group observed desired water flux and salt rejection capacity. Corry et al.[57] studied that functionalized CNT blocks the ions but allows water molecules to pass through the CNTs. Konatham et al.[58] found that both size and chemical functionalization on the rim of the nanopore graphene with various chemical groups ($-COO^-$, $-NH_3^+$, and $-OH$) help to reject the ions. The negatively charged surface of CNT with functional groups ($-COO^-$, $-OH$, and $-CONH_2$) electrostatically favors the adsorption of divalent cations more than the bare CNT without surface charge. The carboxyl group induces more negative charge on the carbon nanotube surface than the other functional groups ($-OH$ and $-CONH_2$). Based on our simulations, the adsorption capacity of divalent metal ions in the presence of the COO^- functional group on the CNT is higher due to the presence of additional oxygen binding site. Hence, the adsorption capacity of all the metal ions (Cd^{2+}, Cu^{2+}, Pb^{2+}, and Hg^{2+}) on functionalized CNT$-COO^-$ (Figure 8) is higher than that seen in the presence of other functional groups ($-OH$ and $-CONH_2$) and bare CNT. The total amount adsorption (q_m) of metal ion on the CNT surface at equilibrium will saturate with an increase in the initial concentration (C_0) of metal ion, as observed in various experimental works.[1,20,32] However, the relative amount of adsorption $\Delta C/C_0$ will decrease with the increase in concentration (C_0) of metal ion in the aqueous system, where ΔC is the difference between the initial and final concentration of metal ion in the solution. The relative amount of adsorption decreases due to the saturation of active adsorption sites of the adsorbent with the metal ions.

Diffusion Coefficient and Occupation Time Distribution Function. The diffusion coefficients of metal ions (Cd^{2+}, Cu^{2+}, and Pb^{2+}) near the CNT surface for different functionalized CNTs are evaluated using the mean square displacement analysis (eqs 5 and 6) and are shown in Figure 9. The behavior of Hg^{2+} is similar to that of other ions studied in this work (figure not shown).The diffusion coefficient values of divalent metals ions within the first coordination shell of ion from the center line of CNT decrease with increasing metal-ion concentrations. The low diffusion coefficient indicates better

Table 2. Parameters of the Langmuir Isotherm Fitted to the Adsorption of Metal Ions on CNT

	estimated Langmuir isotherm parameters							
	CNT		CNT−OH		CNT−$CONH_2$		CNT−COO^-	
metal ion	q_{max} (mmol/g)	K	q_{max} (mmol/g)	K	q_{max} (mmol/g)	K	q_{max} (mmol/g)	K
Pb^{2+}	1.406	2.95	2.07	3.285	1.907	2.914	4.672	7.467
Cu^{2+}	1.219	2.928	1.342	2.984	1.755	2.817	3.565	11.75
Cd^{2+}	1.291	2.772	1.513	3.103	1.563	3.050	3.325	9.817
Hg^{2+}	1.068	2.085	1.284	2.507	1.658	2.573	3.300	3.492

DOI: 10.1021/acs.jpca.5b03352
J. Phys. Chem. A 2015, 119, 8349−8358

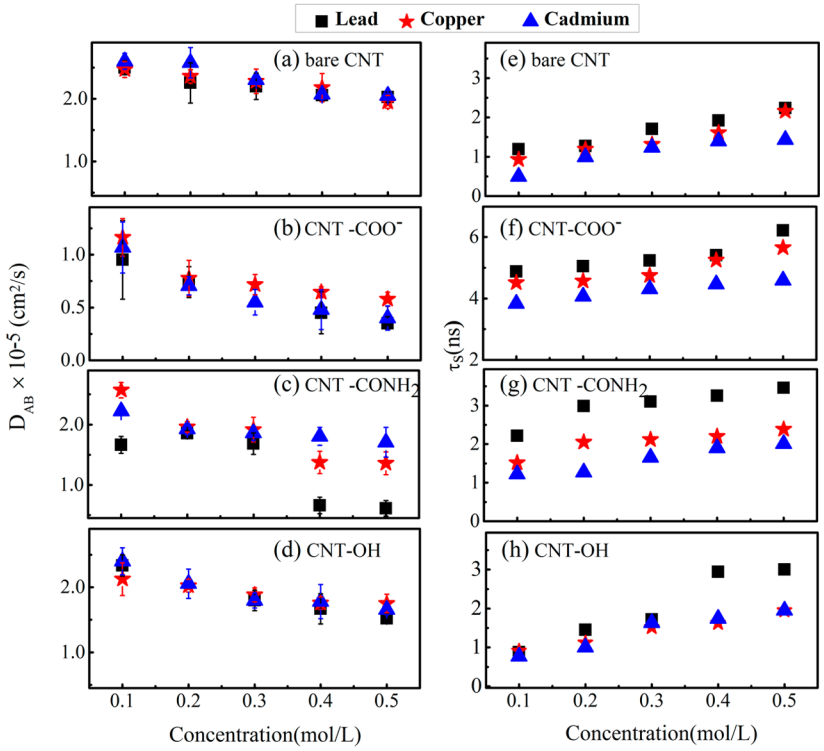

Figure 9. Effect of functional groups on the diffusion coefficient and residence time of metal ions at different concentrations of (a, e) bare CNT, (b, f) CNT−COO^-, (c, g) CNT−$CONH_2$, (d, h) CNT−OH.

adsorption behavior of the metal ion on the CNT surface. The diffusion coefficients of all metal ions are larger, almost at all concentrations, in the presence of bare CNT (Figure 9a), compared to the functionalized CNT (Figure 9b−d). On the contrary, the diffusion coefficient values for all metal ions in the presence of $-COO^-$ functionalized CNT (Figure 9b) are smaller compared to those for −OH and $-CONH_2$ functionalized CNT (Figure 9c,d) and bare CNT. This clearly indicates that the CNT−COO^- is a better adsorbent among all the systems considered in this work. In general, the diffusion coefficient (D) value is smaller for the lead metal ion (Pb^{2+}), for all the considered salt concentrations in this study, than for the other divalent metal ions (Cd^{2+} and Cu^{2+}), which can be primarily associated with the heavy mass of the lead metal ion.

The occupation time distribution function ($R(t)$) is also calculated, which is further used to evaluate the residence time of metal ions in the first coordination shell. The $R(t)$ for all the metal ions (Cd^{2+}, Cu^{2+}, and Pb^{2+}) shows an exponential decay with time. For a given concentration of metal ion, the functionalized CNTs ($-COO^-$, −OH, and $-CONH_2$) show lower decay rates of $R(t)$, indicating a higher residence time of metal ions. The $R(t)$ decay rate is low with increasing concentration and it gives higher value of residence time (τ_s) of metal ions. The residence time of ions for CNT functionalized with different functional groups with increasing ion concentration are shown in Figure 9. Similar to the behavior seen for the diffusivity values, the residence time of ions in the presence of bare CNT is typically lower (Figure 9e) than that seen for functionalized CNTs. On the contrary, the residence time of ions in the presence of $-COO^-$ group functionalized CNT (Figure 9f) is higher compared to the case of the other functional groups (−OH and $-CONH_2$) functionalized on the CNT surface (Figures 9g,h). This is in line with the low diffusion values observed for the $-COO^-$ group functionalized CNT. The lead metal ion (Pb^{2+}) has the high residence time compared to Cu^{2+} and Cd^{2+} ions. The lower value of diffusion coefficient and higher value of residence time of the Pb^{2+} ion further corroborate that it has a higher affinity for adsorption on the CNT surface functionalized with the carboxylic group than on the surface with the hydroxyl and amide functional groups. The larger value of residence time of the metal ion represents a greater affinity toward the functionalized CNT than toward bare CNT. Moreover, functionalized CNTs show a higher τ_s with increasing ion concentration compared to the bare CNT. This implies that the metal-ion adsorption on the functionalized CNT surface is significantly better than the CNT without functionalization that can be further explained using PMF analysis, which is described next.

Potential of Mean Force. The PMF profiles are calculated from the transversely averaged position probabilities, $P(r)$, and defined as $\mathrm{PMF}(r) = -k_B T \ln(P(r))$ and are shown in Figure 10. The PMF profiles of the divalent metal ions in the presence of CNT with and without functionalization have characteristics shape with deep minima. The distinct free energy minima, which we refer to as the PMF value, corresponds to the maximum peak of normalized radial density of metal ions as seen in Figures 2, 4, and 6.

The PMF value for the Cd^{2+} ion is −2.5 kcal/mol for the CNT−COO^-, which is much lower than for bare CNT (∼−0.9 kcal/mol) at 0.1 M concentration, as shown in Figure 10a. At 0.5 M the PMF value for the CNT−COO^- is −1.5 kcal/mol as opposed to ∼−1.0 kcal/mol for bare CNT (Figure 10b). The PMF values for other groups are slightly lower than that of the bare CNT. The lower free energy values indicate favorable adsorption. Hence, at lower concentration the relative affinity for adsorption is much higher, which decreases with the concentration, though the number of ions adsorbed is more at

DOI: 10.1021/acs.jpca.5b03352
J. Phys. Chem. A 2015, 119, 8349−8358

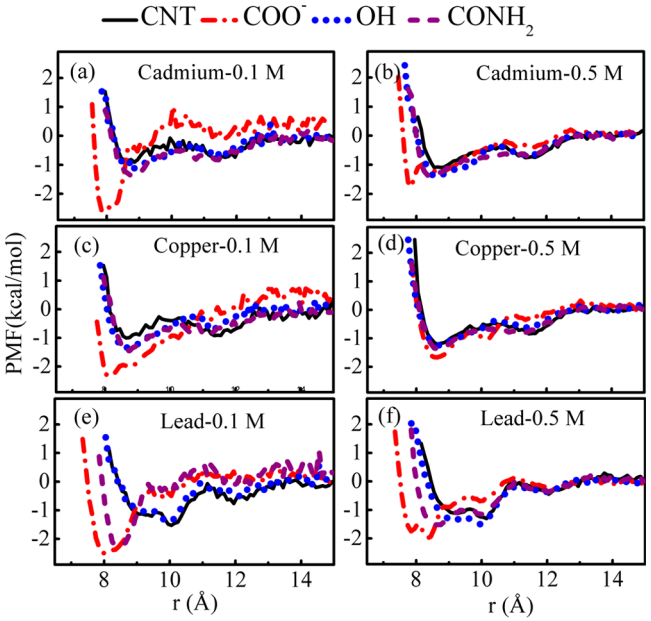

Figure 10. PMF profiles derived from average densities of the metal ions (Cd^{2+}, Cu^{2+}, and Pb^{2+}) in the presence of CNT, with and without functionalization, at (a) 0.1 M and (b) 0.5 M Cd^{2+}; (c) 0.1 M and (d) 0.5 M Cu^{2+}; (e) 0.1 M and (f) 0.5 M Pb^{2+}.

higher concentration until it reaches saturation. The PMF profiles for 0.1 and 0.5 M concentration of Cu^{2+} with functionalized and bare CNT as shown in Figure 10c,d, respectively. The PMF value for Cu^{2+} with functional group ($-COO^-$) on the CNT surface is similar to that seen for Cd^{2+} ion. The PMF profile for Pb^{2+} ion is distinctly different from the other two ions, where the PMF values for CNT$-COO^-$ and CNT$-CONH_2$ systems are almost comparable ∼−2.5 kcal/mol at 0.1 M (Figure 10e). However, the PMF values of CNT−OH and bare CNT are similar, ∼−1 kcal/mol. At 0.5 M with CNT$-COO^-$, the PMF curve of the lead ion shows two deep minimum at ∼8 and 9.5 Å, with the PMF values, −1.6 and −2 kcal/mol, respectively, as shown in Figure 10f. This corresponds to the two density peaks seen in Figure 6e. Interestingly, CNT$-CONH_2$ at 0.5 M (Figure 10f) shows similar adsorption capacity as seen for CNT−OH, though much lower than that of CNT$-COO^-$. It can be seen that metal ions (Pb^{2+}, Cu^{2+}, and Cd^{2+}) have much lower free energy values on average for the CNT functionalized with the carboxylic group ($-COO^-$) compared to the bare and other ($-CONH_2$ and −OH) functionalized CNTs. Similar behavior is seen for the Hg^{2+} ion (figure not shown). Further, the effect of functionalization in adsorption of divalent metal ions on CNT surface is sufficiently high. This effect is stronger in the case of the Pb^{2+} metal ion compared to the Cu^{2+} and Cd^{2+} metal ions. This is attributed to the PMF values of divalent metal ions on the functionalized CNT surface, which follows the order $Pb^{2+} > Cu^{2+} > Cd^{2+}$.

4. CONCLUSION

The adsorption behavior of divalent metal cations (Cd^{2+}, Cu^{2+}, Pb^{2+}, and Hg^{2+}) on a CNT surface is investigated using MD simulations. The normalized radial density profiles of metal ions are calculated with and without functionalized CNT surface ($-COO^-$,−OH, and $-CONH_2$). The number of metal ions adsorbed on the CNT surface is enhanced in the presence of carboxylic ($-COO^-$) functional group compared to the hydroxyl and amide functional groups (−OH and $-CONH_2$) on the CNT surface for five concentrations, viz., 0.1, 0.2, 0.3, 0.4, and 0.5 M. Results from this study showed that the adsorption of heavy metal ions on the CNT surface, with and without functionalization, increases with the increasing concentration of the metal ion in an aqueous solution. The adsorption behavior is well described by the Langmuir isotherm model. The following order of adsorption of heavy metal ions is found: $Pb^{2+} > Cu^{2+} > Cd^{2+} > Hg^{2+}$, which is well supported by the PMF calculations. In general, CNT with functionalization of carboxylic group ($-COO^-$) is a better adsorbent than other functional groups (−OH and $-CONH_2$).

AUTHOR INFORMATION

Corresponding Author

*J. K. Singh. E-mail: jayantks@iitk.ac.in. Telephone no.: 91-512-259 6141.

Notes

The authors declare no competing financial interest.

ACKNOWLEDGMENTS

This work is supported by the Department of Atomic Energy, Government of India. The computational resources are provided by the HPC, Computer Center (CC), Indian Institute of Technology Kanpur.

REFERENCES

(1) Al-Degs, Y. S.; El-Barghouthi, M. I.; Issa, A. A.; Khraisheh, M. A.; Walker, G. M. Sorption of Zn(II), Pb(II), and Co(II) Using Natural Sorbents: Equilibrium and Kinetic Studies. *Water Res.* **2006**, *40*, 2645−2658.

(2) Wang, Z.; Yin, P.; Wang, Z.; Qu, R.; Liu, X. Chelating Resins Silica Gel Supported Aminophosphonic Acids Prepared by a Heterogeneous Synthesis Method and a Homogeneous Synthesis Method and the Removal Properties for Hg(II) from Aqueous Solutions. *Ind. Eng. Chem. Res.* **2012**, *51*, 8598−8607.

(3) Wang, Z.; Yin, P.; Wang, Z.; Xu, Q.; Qu, R.; Tang, Q. Removal of Pb(II) and Cu(II) Ions from Aqueous Solutions by Manganese Phosphonate. *Sep. Sci. Technol.* **2012**, *48*, 281−287.

(4) Zolfaghari, G.; Esmaili-Sari, A.; Anbia, M.; Younesi, H.; Ghasemian, M. B. A Zinc Oxide-Coated Nanoporous Carbon Adsorbent for Lead Removal from Water: Optimization, Equilibrium Modeling, and Kinetics Studies. *Int. J. Environ. Sci. Technol.* **2013**, *10*, 325−340.

(5) Ho, Y. S.; Huang, C. T.; Huang, H. W. Equilibrium Sorption Isotherm for Metal Ions on Tree Fern. *Process Biochem.* **2002**, *37*, 1421−1430.

(6) Srivastava, V. C.; Mall, I. D.; Mishra, I. M. Characterization of Mesoporous Rice Husk Ash (RHA) and Adsorption Kinetics of Metal Ions from Aqueous Solution onto RHA. *J. Hazard. Mater.* **2006**, *134*, 257−267.

(7) Peterson, G. W.; Rossin, J. A.; Smith, P. B.; Wagner, G. W. Effects of Water on the Removal of Methyl Bromide Using Triethylene Diamine Impregnated Carbon. *Carbon* **2010**, *48*, 81−88.

(8) Chen, Q.; Luo, Z.; Hills, C.; Xue, G.; Tyrer, M. Precipitation of Heavy Metals from Wastewater Using Simulated Flue Gas: Sequent Additions of Fly Ash, Lime and Carbon Dioxide. *Water Res.* **2009**, *43*, 2605−2614.

(9) Alvarez, M. T.; Crespo, C.; Mattiasson, B. Precipitation of Zn(II), Cu(II) and Pb(II) at Bench-Scale Using Biogenic Hydrogen Sulfide from the Utilization of Volatile Fatty Acids. *Chemosphere* **2007**, *66*, 1677−1683.

(10) Kongsricharoern, N.; Polprasert, C. Electrochemical Precipitation of Chromium (Cr^{6+}) from an Electroplating Wastewater. *Water Sci. Technol.* **1995**, *31*, 109−117.

DOI: 10.1021/acs.jpca.5b03352
J. Phys. Chem. A 2015, 119, 8349−8358

(11) Inglezakis, V. J.; Grigoropoulou, H. P. Modeling of Ion Exchange of Pb^{2+} in Fixed Beds of Clinoptilolite. *Microporous Mesoporous Mater.* **2003**, *61*, 273−282.
(12) Inglezakis, V. J.; Stylianou, M. A.; Gkantzou, D.; Loizidou, M. D. Removal of Pb(II) from Aqueous Solutions by Using Clinoptilolite and Bentonite as Adsorbents. *Desalination* **2007**, *210*, 248−256.
(13) Berber-Mendoza, M. S.; Leyva-Ramos, R.; Alonso-Davila, P.; Fuentes-Rubio, L.; Guerrero-Coronado, R. M. Comparison of Isotherms for the Ion Exchange of Pb(II) from Aqueous Solution onto Homoionic Clinoptilolite. *J. Colloid Interface Sci.* **2006**, *301*, 40−45.
(14) Ferella, F.; Prisciandaro, M.; De Michelis, I.; Veglio', F. Removal of Heavy Metals by Surfactant-Enhanced Ultrafiltration from Wastewaters. *Desalination* **2007**, *207*, 125−133.
(15) Huang, J.-H.; Zeng, G.-M.; Zhou, C.-F.; Li, X.; Shi, L.-J.; He, S.-B. Adsorption of Surfactant Micelles and Cd^{2+}/Zn^{2+} in Micellar-Enhanced Ultrafiltration. *J. Hazard. Mater.* **2010**, *183*, 287−293.
(16) Jellouli Ennigrou, D.; Gzara, L.; Ramzi Ben Romdhane, M.; Dhahbi, M. Cadmium Removal from Aqueous Solutions by Polyelectrolyte Enhanced Ultrafiltration. *Desalination* **2009**, *246*, 363−369.
(17) Zhu, B.-J.; Yu, X.-Y.; Jia, Y.; Peng, F.-M.; Sun, B.; Zhang, M.-Y.; Luo, T.; Liu, J.-H.; Huang, X.-J. Iron and 1,3,5-Benzenetricarboxylic Metal-Organic Coordination Polymers Prepared by Solvothermal Method and Their Application in Efficient As(V) Removal from Aqueous Solutions. *J. Phys. Chem. C* **2012**, *116*, 8601−8607.
(18) Fu, F.; Wang, Q. Removal of Heavy Metal Ions from Wastewaters: A Review. *J. Environ. Manage.* **2011**, *92*, 407−418.
(19) Wang, H.; Zhou, A.; Peng, F.; Yu, H.; Yang, J. Mechanism Study on Adsorption of Acidified Multiwalled Carbon Nanotubes to Pb(II). *J. Colloid Interface Sci.* **2007**, *316*, 277−283.
(20) Kabbashi, N. A.; Atieh, M. A.; Al-Mamun, A.; Mirghami, M. E. S.; Alam, M. D. Z.; Yahya, N. Kinetic Adsorption of Application of Carbon Nanotubes for Pb(II) Removal from Aqueous Solution. *J. Environ. Sci. (Beijing, China)* **2009**, *21*, 539−544.
(21) Kuo, C.-Y.; Lin, H.-Y. Adsorption of Aqueous Cadmium (II) onto Modified Multi-Walled Carbon Nanotubes Following Microwave/Chemical Treatment. *Desalination* **2009**, *249*, 792−796.
(22) Pillay, K.; Cukrowska, E. M.; Coville, N. J. Multi-Walled Carbon Nanotubes as Adsorbents for the Removal of Parts Per Billion Levels of Hexavalent Chromium from Aqueous Solution. *J. Hazard. Mater.* **2009**, *166*, 1067−1075.
(23) Li, Y.; Liu, F.; Xia, B.; Du, Q.; Zhang, P.; Wang, D.; Wang, Z.; Xia, Y. Removal of Copper from Aqueous Solution by Carbon Nanotube/Calcium Alginate Composites. *J. Hazard. Mater.* **2010**, *177*, 876−880.
(24) Kandah, M. I.; Meunier, J.-L. Removal of Nickel Ions from Water by Multi-Walled Carbon Nanotubes. *J. Hazard. Mater.* **2007**, *146*, 283−288.
(25) Odom, T. W.; Huang, J.-L.; Kim, P.; Lieber, C. M. Atomic Structure and Electronic Properties of Single-Walled Carbon Nanotubes. *Nature* **1998**, *391*, 62−64.
(26) Balkanski, M. *Physical Properties of Carbon Nanotubes*; Saito, R., Dresselhaus, G., Dresselhaus, M. S., Eds.; Imperial College Press: London, 1998. *Mater. Sci. Eng., B* **2000**, *76*, 241−242, DOI: 10.1016/S0921-5107(00)00444-X.
(27) Lu, C.; Chiu, H.; Liu, C. Removal of Zinc(II) from Aqueous Solution by Purified Carbon Nanotubes: Kinetics and Equilibrium Studies. *Ind. Eng. Chem. Res.* **2006**, *45*, 2850−2855.
(28) Rao, G. P.; Lu, C.; Su, F. Sorption of Divalent Metal Ions from Aqueous Solution by Carbon Nanotubes: A Review. *Sep. Purif. Technol.* **2007**, *58*, 224−231.
(29) Li, Y.-H.; Wang, S.; Luan, Z.; Ding, J.; Xu, C.; Wu, D. Adsorption of Cadmium (II) from Aqueous Solution by Surface Oxidized Carbon Nanotubes. *Carbon* **2003**, *41*, 1057−1062.
(30) Chingombe, P.; Saha, B.; Wakeman, R. J. Surface Modification and Characterisation of a Coal-Based Activated Carbon. *Carbon* **2005**, *43*, 3132−3143.
(31) Biniak, S.; Pakuła, M.; Szymański, G. S.; Świątkowski, A. Effect of Activated Carbon Surface Oxygen- and/or Nitrogen-Containing Groups on Adsorption of Copper(II) Ions from Aqueous Solution. *Langmuir* **1999**, *15*, 6117−6122.
(32) Moradi, O.; Zare, K.; Monajjemi, M.; Yari, M.; Aghaie, H. The Studies of Equilibrium and Thermodynamic Adsorption of Pb(II), Cd(II) and Cu(II) Ions from Aqueous Solution onto Swcnts and Swcnt-Cooh Surfaces. *Fullerenes, Nanotubes, Carbon Nanostruct.* **2010**, *18*, 285−302.
(33) Lu, C.; Chiu, H. Adsorption of Zinc(II) from Water with Purified Carbon Nanotubes. *Chem. Eng. Sci.* **2006**, *61*, 1138−1145.
(34) Li, Y.-H.; Zhu, Y.; Zhao, Y.; Wu, D.; Luan, Z. Different Morphologies of Carbon Nanotubes Effect on the Lead Removal from Aqueous Solution. *Diamond Relat. Mater.* **2006**, *15*, 90−94.
(35) Liang, P.; Liu, Y.; Guo, L.; Zeng, J.; Lu, H. Multiwalled Carbon Nanotubes as Solid-Phase Extraction Adsorbent for the Preconcentration of Trace Metal Ions and Their Determination by Inductively Coupled Plasma Atomic Emission Spectrometry. *J. Anal. At. Spectrom.* **2004**, *19*, 1489−1492.
(36) Li, Y.-H.; Di, Z.; Ding, J.; Wu, D.; Luan, Z.; Zhu, Y. Adsorption Thermodynamic, Kinetic and Desorption Studies of Pb2+ on Carbon Nanotubes. *Water Res.* **2005**, *39*, 605−609.
(37) Sheng, G.; Li, J.; Shao, D.; Hu, J.; Chen, C.; Chen, Y.; Wang, X. Adsorption of Copper(II) on Multiwalled Carbon Nanotubes in the Absence and Presence of Humic or Fulvic Acids. *J. Hazard. Mater.* **2010**, *178*, 333−340.
(38) El-Sheikh, A. H.; Al-Degs, Y. S.; Al-Asad, R. M.; Sweileh, J. A. Effect of Oxidation and Geometrical Dimensions of Carbon Nanotubes on Hg(II) Sorption and Preconcentration from Real Waters. *Desalination* **2011**, *270*, 214−220.
(39) Wang, H. J.; Zhou, A. L.; Peng, F.; Yu, H.; Chen, L. F. Adsorption Characteristic of Acidified Carbon Nanotubes for Heavy Metal Pb(II) in Aqueous Solution. *Mater. Sci. Eng., A* **2007**, *466*, 201−206.
(40) Pyrzynska, K.; Bystrzejewski, M. Comparative Study of Heavy Metal Ions Sorption onto Activated Carbon, Carbon Nanotubes, and Carbon-Encapsulated Magnetic Nanoparticles. *Colloids Surf., A* **2010**, *362*, 102−109.
(41) Ansari, A.; Mehrabian, M. A.; Hashemipour, H. Zinc Ion Adsorption on Carbon Nanotubes in an Aqueous Solution. *Pol. J. Chem. Technol.* **2012**, *14*, 29.
(42) Ansari Dezfoli, A. R.; Mehrabian, M. A.; Hashemipour, H. Comparative Study of Zn(II) and Cd(Ii) Ions Adsorption on Charged Carbon Nano Tubes: Molecular Dynamics Approach. *Adsorption* **2013**, *19*, 1253−1261.
(43) Dezfoli Ansari, A. R. A.; Mehrabian, M. A.; Hashemipour, H. Study of Interaction Energies in Zinc Ion Adsorption on Charged Carbon Nano-Tubes Using Molecular Dynamics Simulation. *J. Comput. Theor. Nanosci.* **2013**, *10*, 2411−2417.
(44) Jorgensen, W. L.; Chandrasekhar, J.; Madura, J. D.; Impey, R. W.; Klein, M. L. Comparison of Simple Potential Functions for Simulating Liquid Water. *J. Chem. Phys.* **1983**, *79*, 926−935.
(45) Jorgensen, W. L.; Maxwell, D. S.; Tirado-Rives, J. Development and Testing of the Opls All-Atom Force Field on Conformational Energetics and Properties of Organic Liquids. *J. Am. Chem. Soc.* **1996**, *118*, 11225−11236.
(46) Huang, L.-L.; Shao, Q.; Lu, L.-H.; Lu, X.-H.; Zhang, L.-Z.; Wang, J.; Jiang, S.-y. Helicity and Temperature Effects on Static Properties of Water Molecules Confined in Modified Carbon Nanotubes. *Phys. Chem. Chem. Phys.* **2006**, *8*, 3836−3844.
(47) Allen, M. P.; Tildesley, D. J. *Computer Simulation of Liquids*; Oxford University Press: Oxford, U.K., 1987.
(48) Hummer, G.; Rasaiah, J. C.; Noworyta, J. P. Water Conduction through the Hydrophobic Channel of a Carbon Nanotube. *Nature* **2001**, *414*, 188−190.
(49) Xiu, P.; Zhou, B.; Qi, W.; Lu, H.; Tu, Y.; Fang, H. Manipulating Biomolecules with Aqueous Liquids Confined within Single-Walled Nanotubes. *J. Am. Chem. Soc.* **2009**, *131*, 2840−2845.

DOI: 10.1021/acs.jpca.5b03352
J. Phys. Chem. A 2015, 119, 8349−8358

(50) Xiu, P.; Yang, Z.; Zhou, B.; Das, P.; Fang, H.; Zhou, R. Urea-Induced Drying of Hydrophobic Nanotubes: Comparison of Different Urea Models. *J. Phys. Chem. B* **2011**, *115*, 2988−2994.
(51) Xiu, P.; Tu, Y.; Tian, X.; Fang, H.; Zhou, R. Molecular Wire of Urea in Carbon Nanotube: A Molecular Dynamics Study. *Nanoscale* **2012**, *4*, 652−658.
(52) Yang, Z.; Wang, Z.; Tian, X.; Xiu, P.; Zhou, R. Amino Acid Analogues Bind to Carbon Nanotube Via Π-Π Interactions: Comparison of Molecular Mechanical and Quantum Mechanical Calculations. *J. Chem. Phys.* **2012**, *136*, 025103.
(53) Plimpton, S. Fast Parallel Algorithms for Short-Range Molecular Dynamics. *J. Comput. Phys.* **1995**, *117*, 1−19.
(54) Martínez, L.; Andrade, R.; Birgin, E. G.; Martínez, J. M. Packmol: A Package for Building Initial Configurations for Molecular Dynamics Simulations. *J. Comput. Chem.* **2009**, *30*, 2157−2164.
(55) Hoover, W. G. Canonical Dynamics: Equilibrium Phase-Space Distributions. *Phys. Rev. A: At., Mol., Opt. Phys.* **1985**, *31*, 1695−1697.
(56) Nosé, S. A Unified Formulation of the Constant Temperature Molecular Dynamics Methods. *J. Chem. Phys.* **1984**, *81*, 511−519.
(57) Corry, B. Water and Ion Transport through Functionalised Carbon Nanotubes: Implications for Desalination Technology. *Energy Environ. Sci.* **2011**, *4*, 751−759.
(58) Konatham, D.; Yu, J.; Ho, T. A.; Striolo, A. Simulation Insights for Graphene-Based Water Desalination Membranes. *Langmuir* **2013**, *29*, 11884−11897.

DOI: 10.1021/acs.jpca.5b03352
J. Phys. Chem. A 2015, 119, 8349−8358